ACS Catalysis

Research Article

pubs.acs.org/acscatalysis

Role of Delamination in Zeolite-Catalyzed Aromatic Alkylation: UCB-3 versus 3-D Al-SSZ-70

Ron C. Runnebaum,[†] Xiaoying Ouyang,[†] Jeffrey A. Edsinga,[†,⊥] Thomas Rea,[∥] Ilke Arslan,[‡] Son-Jong Hwang,[§] Stacey I. Zones,*[,†,∥] and Alexander Katz*[,†]

[†]Department of Chemical and Biomolecuar Engineering, University of California, Berkeley, California 94720, United States

[‡]Pacific Northwest National Laboratory, Richland, Washington 99352, United States

[§]Division of Chemistry and Chemical Engineering, California Institute of Technology, Pasadena, California 91125, United States

[∥]Chevron Energy Technology Company, Richmond, California 94804, United States

Supporting Information

ABSTRACT: Delaminated zeolite UCB-3 exhibits 2.4-fold greater catalytic activity relative to its three-dimensional (3D) zeolite counterpart, Al-SSZ-70, and 2.0-fold greater activity (per catalyst mass) when compared with industrial catalyst MCM-22, for the alkylation of toluene with propylene at 523 K. The former increase is nearly equal to the observed relative increase in external surface area and acid sites upon delamination. However, at 423 K for the same reaction, UCB-3 exhibits a 3.5-fold greater catalytic activity relative to 3D Al-SSZ-70. The higher relative rate enhancement for the delaminated material at lower temperature can be elucidated on the basis of increased contributions from internal acid sites. Evidence of possible contributions from such acid sites is obtained by performing catalysis after silanation treatment, which demonstrates that although virtually all catalysis in MCM-22 occurs on the external surface, catalysis also occurs on internal sites for 3D Al-SSZ-70. The additional observed enhancement at low temperatures can therefore be rationalized by greater access to internal active sites as a result of sheet breakage during delamination. Such breakage leads to shorter characteristic internal diffusion paths and was visualized using TEM comparisons of UCB-3 and 3D Al-SSZ-70.

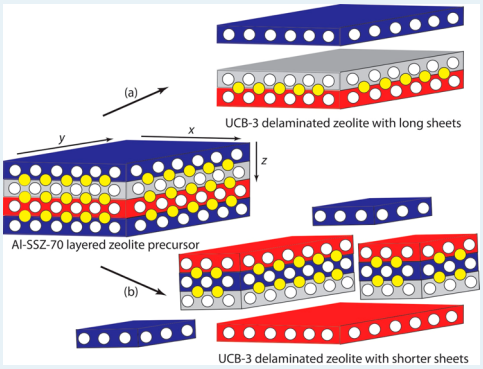

KEYWORDS: *delamination, exfoliation, layered zeolite precursor, SSZ-70, MCM-22, aromatic alkylation, cymene, cumene*

Zeolites' crystallinity enables high densities of uniform and well-defined acid sites, which are impossible to achieve with amorphous silica–alumina materials and are useful as solid-acid catalysts for a number of reaction classes, including isomerization, dehydration, and alkylation.[1,2] Although virtually all of the microporous surface area of the zeolite can be available for catalysis when the size of the reactants is relatively small (isomerization of 1-hexene,[3] or alkylation of benzene with methanol to form *p*-xylene[4]), in many other instances, the sterics of the zeolite framework severely limits where catalysis can occur.[5−7] Such is the case in aromatic alkylation with C3 and larger olefins, when using MWW-type zeolites such as MCM-22, which are industrial solid-acid catalysts for aromatic alkylation. Only a small fraction of the total number of acid sites is typically invoked as being active under reaction conditions: those located in the immediate vicinity of the external surface.[3,8−12] Delamination of MWW-type layered zeolite precursors aims to synthesize catalysts with an increased density of external-surface acid sites,[13−18] and there has been a conscious effort to perform this delamination under mild conditions that preserve the integrity of the two-dimensional zeolite sheets.[19,20] This leads to higher reaction rates and less deactivation for aromatic alkylation reactions,[17] which has been presumed to arise from the increased external surface area of the delaminated material, as shown in Figure 1a.

Here, in this manuscript, we demonstrate a different mechanism by which delamination increases the rate of zeolite-catalyzed reactions, due to breakage of sheets into smaller pieces in a direction perpendicular to delamination. In a MWW-type layered material, delamination occurs parallel to the two nonintersecting micropore channels that are used for molecular transport via diffusion,[16] as represented by the x−y plane of Figure 1. Because delamination is parallel to the direction of internal transport, the conventional belief has been that the benefit of delamination of MWW-type layered materials on the reaction rate is limited to only external acid-site density effects. However, we demonstrate that sheet breakage along the x and y directions accompanies delamination, as shown in Figure 1b, and this breakage leads to higher rates of diffusive transport to internal acid sites by decreasing the characteristic diffusion-path length along internal microporous channels. We provide evidence of such a mechanism

Received: March 13, 2014
Revised: May 19, 2014
Published: June 3, 2014

   dx.doi.org/10.1021/cs500285w | ACS Catal. 2014, 4, 2364−2368

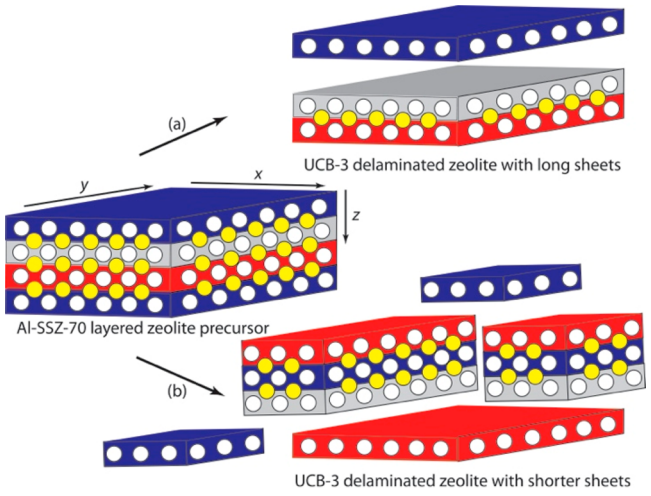

Figure 1. Schematic representation of two possible benefits of Al-SSZ-70 delamination: (a) conventional benefit consisting of separated long sheets and (b) proposed new benefit of delamination, in which UCB-3 delaminated zeolite consists of shorter sheets formed by the breakage of layers during delamination. White circles indicate 10-MR openings to intralayer sinusoidal micropore channels, and yellow circles indicate openings to interlayer micropore channels containing supercages.

operating in a working delaminated zeolite solid-acid catalyst system. Our approach uses zeolite SSZ-70, which, although crystallographically and catalytically distinct from MCM-22, has several structural features similar to MWW-type zeolites (e.g., MCM-22) in that it is also a layered-zeolite precursor consisting of lamellae in the as-synthesized state.[21,22] We delaminate Al-SSZ-70 under nonaqueous conditions using fluoride anion to synthesize UCB-3, which results in heteroatom retention, a lack of amorphization of the zeolite framework, and a higher density of external acid sites on a per-mass basis, and compare the catalytic activity and selectivity of UCB-3 and its three-dimensional Al-SSZ-70 zeolite counterpart, using alkylation of toluene with propylene as a probe reaction. In MWW-type zeolite-catalyzed reactions, such as alkylation of benzene with propylene, ITQ-2 (the delaminated MWW counterpart to MCM-22) has been reported to deactivate less and therefore achieves a higher rate of cumene production with longer times on stream relative to its three-dimensional counterpart, MCM-22.[17] Our goal is to study whether delamination also leads to catalytic rate enhancements for UCB-3 versus Al-SSZ-70 and how the relative catalytic rates of these two materials scale with each other at different temperatures. High-temperature catalysis data highlights the benefit of the previously reported[23] increased external surface area per mass of catalyst upon delamination. In contrast, low-temperature catalysis data inform regarding the possible role of decreased characteristic path length for internal diffusion (i.e., shorter sheets) as a result of breakage of sheets during delamination.

To further support the observed catalytic enhancements due to internal and external acid sites described above, we used TEM (transmission electron microscopy) to visualize broken sheets and external-surface silanation to prove the catalytic significance and greater accessibility of acid sites located within internal micropores, when using UCB-3.

We synthesized UCB-3 via delamination of Al-SSZ-70 using published procedures.[23] Our materials characterization data are summarized in Table 1 (with details that reproduce previously published characterization data for Al-SSZ-70 and UCB-3 in the Supporting Information) and demonstrate a 2-fold increase in external surface area upon delamination, when comparing calcined UCB-3 with its three-dimensional (3D) zeolite counterpart (calcined Al-SSZ-70). We titrated the external surface area with bulky base molecules to investigate the relative density of external acid sites. When using acridine (at room temperature) and 2,4,6-trimethylpyridine (collidine, at 423 K) as titrants, calcined UCB-3 exhibited a 1.8-fold and 1.3-fold higher uptake relative to 3D Al-SSZ-70, respectively. The slight discrepancy between collidine and acridine uptakes may be the result of neighboring acid sites, which are titrated to varying extents by the bulky amine probes on the basis of sterics. Altogether, the data above support an increase in external surface area and density of external acid sites upon Al-SSZ-70 delamination. These data are consistent with Figure 1a and the greater degree of layer separation upon delamination that is observed using HAADF-STEM (Supporting Information Figure S1).

To understand the catalytic consequences of delamination, we compared calcined UCB-3 and 3D Al-SSZ-70 as catalysts for toluene alkylation with propylene at various temperatures. Data shown in Figure 2a represent toluene alkylation rate versus time-on-stream for a once-through packed-bed flow reactor at 523 K. Calcined UCB-3 exhibited a 2.4-fold increase in reaction rate when extrapolated to zero time-on-stream relative to 3D Al-SSZ-70 under the same reaction conditions. This is nearly equal to the increase in external-surface area accompanying delamination and can therefore be rationalized by the increase in external acid site density according to Figure 1a (vide supra). We compared the selectivity profiles of each catalyst for the three major products (*ortho*-, *meta*-, and *para*-cymene isomers) by using cross-plots in Figure 2, which are graphical representations of the product isomer distribution of one catalyst on one set of orthogonal axes plotted versus another catalyst on the other set of axes. A linear trend in the

Table 1. Material and Catalytic Characterization Data of Calcined UCB-3, Calcined Al-SSZ-70, and Calcined Al-MCM-22, Including External-Surface Area As Measured by N_2 Physisorption, Total and External Brønsted Acid Sites As Measured by Amine Chemisorption, and Overall Reaction Rate

				external acid sites measured by bulky amines, μmol/g		rate of reaction at various temperatures,[d] mol (g of catalyst)$^{-1}$ h^{-1}	
sample	Si/Al	$S_{external}$,[a] m^2/g	total acid sites measured by pyridine adsorption,[b] μmol/g	collidine[b]	acridine[c]	423 K	523 K
Al-SSZ-70	40	100	299	135	140	0.031	0.082
UCB-3	40	190	257	170	252	0.108	0.198
MCM-22	25	60	512	70	81		0.101

[a]determined by *t*-plot method; thickness range 0.4−0.6 nm. [b]measured by TGA. [c]measured by UV−vis. [d]rate of reaction at zero time-on-stream.

dx.doi.org/10.1021/cs500285w | ACS Catal. 2014, 4, 2364−2368

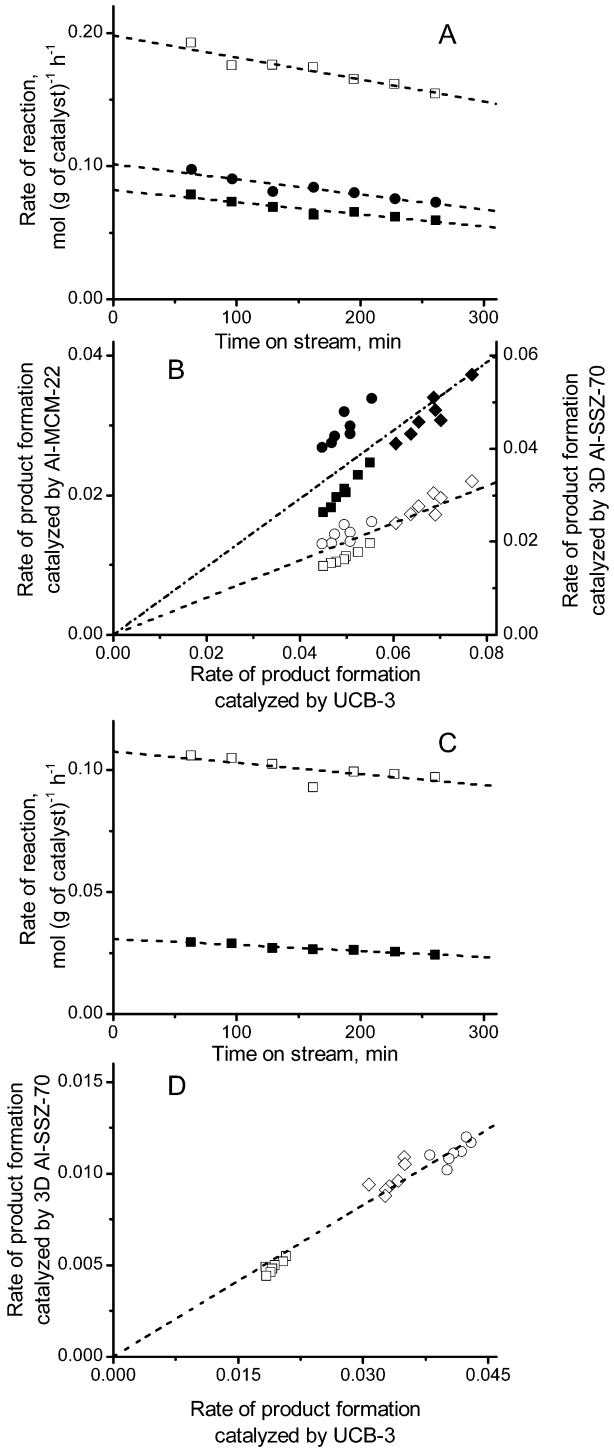

Figure 2. Rate of toluene conversion catalyzed by UCB-3 (□), Al-SSZ-70 (■), and Al-MCM-22 (●) as a function of time-on-stream at 523 K (A) and 423 K (C). Cross-plots show the rates of product formation at 523 K (B) and 423 K (D) at various times-on-stream. Closed symbols characterize Al-MCM-22 versus UCB-3: *m*- (■), *p*- (◆), and *o*- (●) cymene. Open symbols characterize Al-SSZ-70 versus UCB-3: *m*- (□), *p*- (◊), and *o*- (○) cymene. Rates are in units of mol (g of catalyst)$^{-1}$ h^{-1}. Additional comparison data at 473 K are located in the Supporting Information (Figure S7 and Table S1).

cross-plot results from an identical product selectivity distribution for the two catalysts being compared (i.e., when the absolute rates for forming an isomer product are different by the same factor on the two catalysts being compared, for all isomer products). Data in Figure 2b demonstrate relatively high ortho and low meta selectivities for both UCB-3 and 3D Al-SSZ-70, which have also been observed in other reaction systems, such as the analogous Friedel−Crafts aromatic alkylation.[24,25] The linearity of these data demonstrates a lack of any significant selectivity differences between UCB-3 and 3D Al-SSZ-70.

Upon decreasing reaction temperature to 423 K in Figure 2c, calcined UCB-3 is 3.5-fold more active relative to Al-SSZ-70 while showing a similar selectivity profile for the various product isomers in Figure 2d. Figure 3 shows the overall trend

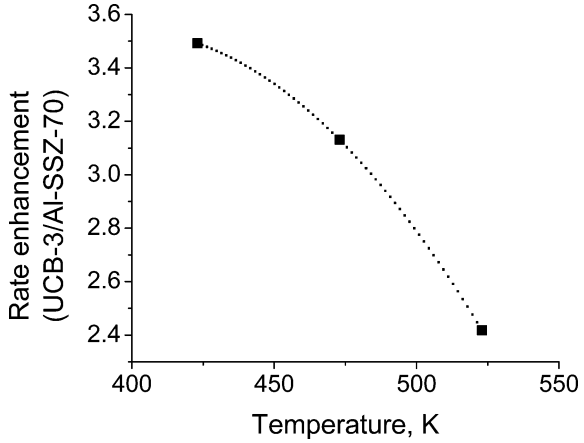

Figure 3. Rate enhancement (reaction rate of UCB-3 divided by reaction rate of Al-SSZ-70) decreases as a function of temperature, which is expected as internal diffusion becomes less significant at increasing temperatures relative to reaction rate. The dashed trendline is for visual clarity.

at all reaction temperatures investigated and demonstrates an increasing relative-rate enhancement upon delamination as temperature decreases. If the only reason for the observed rate enhancement upon delamination was an increase in the density of external acid sites, as shown in Figure 1a, the relative rate enhancement should be fixed and not change significantly with reaction temperature. Instead, the increase in observed relative rate enhancement for UCB-3 over Al-SSZ-70 in Figure 3 at lower temperatures indicates that an additional mechanism for catalysis rate enhancement upon delamination must exist, which is not entirely captured by Figure 1a.

We hypothesized that internal acid sites could be key to understanding the additional observed rate enhancement for UCB-3 over Al-SSZ-70, at temperatures below 523 K in Figure 3. Our rationale was that at 523 K, the large value of the Thiele modulus led to an effectiveness factor that was low and dominated by the number density of external acid sites (vide supra) rather than internal-site contributions. However, we further hypothesized that sheet fragmentation in UCB-3 could lead to even higher relative rates over Al-SSZ-70 as the temperature was lowered from 523 K in Figure 3. This is because at these lower temperatures, the contribution from internal acid sites is more significant, and the internal diffusion path for these sheets is shorter in UCB-3 relative to Al-SSZ-70 as a result of sheet fragmentation in the former (vide infra). Indeed, according to classical treatments of coupled reaction and mass transport in porous catalyst particles, the transport-limited observed rate of internal catalyst sites is inversely proportional to the size of the catalyst particle along the

dx.doi.org/10.1021/cs500285w | ACS Catal. 2014, 4, 2364−2368

diffusion path and has an activation energy of one-half of the true kinetic activation energy.[29] The latter mathematically justifies why the contribution of internal acid sites is more pronounced at lower temperatures because external acid sites function at the true kinetic activation energy (in the absence of external-transport restrictions) and because lowering the temperature in general tends to disproportionately increase the rate of the process with the lower activation energy.

To support the hypothesis above, TEM micrographs in Figure 4 compare the morphology of as-made Al-SSZ-70 and

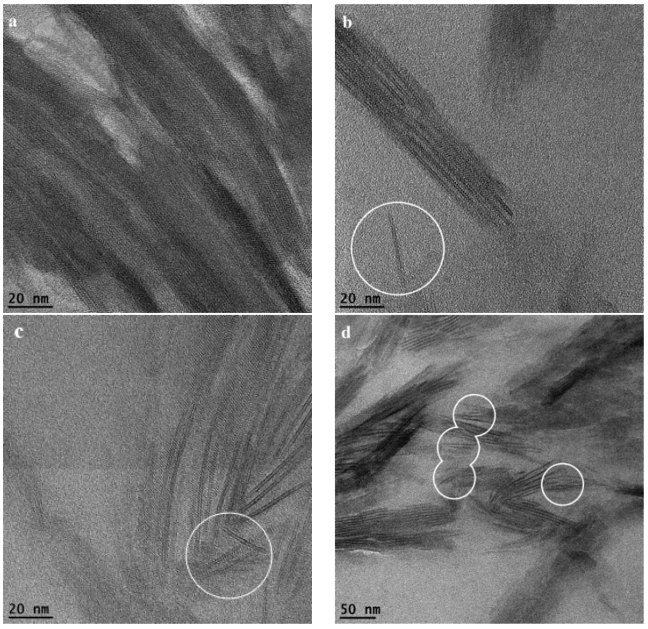

Figure 4. TEM images characterizing (a) as-made Al-SSZ-70 precursor and (b–d) UCB-3 delaminated zeolite. Both materials are uncalcined. The circles indicate the presence of shorter sheets that are evident in the UCB-3 images.

UCB-3. These data demonstrate long rectilinear sheets that break into smaller fragments upon delamination. Circles highlight fragmented sheets in as-made UCB-3, which are not observed in as-made Al-SSZ-70 in Figure 4. This observed sheet breakage provides a heretofore unrecognized route by which delamination enhances catalysis by effectively providing a shorter diffusion path length to interior acid sites. Such a mechanism of enhancing catalysis via delamination is schematically represented in Figure 1b and implicitly assumes that internal acid sites are catalytically accessible and active.

To determine the extent to which internal acid sites contribute to catalysis under our reaction conditions, we silanated 3D Al-SSZ-70 and compared the catalyzed reaction rates before and after silanation. The silanation deposition procedure has been previously shown to poison external acid sites active in ZSM-5-catalyzed alkylation and disproportionation.[26−28] We observed a lack of significant decrease in the microporosity of the silanated Al-SSZ-70 as compared with the parent Al-SSZ-70 material before silanation (Supporting Information (SI) Table S2). These data are consistent with lack of internal micropore blockage upon silanation. If the alkylation of toluene with propylene occurs primarily on the external surface of 3D Al-SSZ-70, silanation of its external surface should almost completely shut down catalytic activity. However, the catalytic activity (alkylation of toluene with propylene at 523 K) decreased by 2.5-fold as a result of silanation of 3D Al-SSZ-70 (in SI Table S2). Although this result is consistent with our assertion of mainly external acid sites performing catalysis at 523 K, it also demonstrates an extraordinarily high contribution of internal acid sites to the overall catalysis rate in Al-SSZ-70. As a comparison, we also silanated Al-MCM-22 and compared the catalytic activity of silanated versus unsilanated Al-MCM-22 at 523 K upon also confirming a lack of micropore blockage due to silanation (SI Table S2). The reaction rate of Al-MCM-22 decreased by at least 10-fold as a result of the silanation (SI Table S2). Such a result is consistent with previous reports of lack of significant internal-site participation in Al-MCM-22 during aromatic alkylation catalysis.[3,8,10] These results demonstrate that internal acid sites can be active participants in the alkylation of toluene with propylene as catalyzed by Al-SSZ-70 but likely do not contribute significantly for the same reaction and conditions in Al-MCM-22. Though these data reinforce Al-SSZ-70 being distinct from Al-MCM-22, while currently lacking a structure for the former, it is impossible to hypothesize the molecular-scale features that may be responsible for these observed differences.

In summary, the data above support our hypothesis of why there is additional catalytic rate enhancement for UCB-3 relative to Al-SSZ-70 as temperature is lowered below 523 K in Figure 3. This rate enhancement for UCB-3 results from a combination of internal acid sites becoming significant contributors to the overall rate at lower temperatures as well as sheet fragmentation in the $a-b$ plane during delamination, which was observed via TEM in Figure 4. In conjunction with results of Archer et al.[21] and Guisnet et al.,[10] we hypothesize that these internal sites may be located within supercages, which are represented by the yellow pore system of Figure 1. Our results also indicate that external acid-site contributions are the significant ones at higher temperatures in Figure 3, and these sites appear to be the same across samples,[30] as previously demonstrated for self-pillared zeolite nanosheets, because our relative activity between samples at higher temperatures scales with measured external surface area.

Having demonstrated benefits of delamination, as shown by the distinct mechanisms schematically represented by Figure 1a and 1b, we compare the catalytic activity of UCB-3 with an industrial catalyst, Al-MCM-22, both of which are summarized in Table 1. UCB-3 exhibited a 2-fold increase in catalytic activity, which is all the more impressive given the mass-basis used for comparing activity in Figure 2 and given the higher Si/Al ratio of UCB-3 (i.e., when using an acid site rather than mass basis, the activity enhancement for UCB-3 over Al-MCM-22 is further enlarged by an additional 2-fold relative to values reported above). UCB-3 and Al-MCM-22 exhibited similar selectivities to *m*-, *p*-, and *o*-cymene at 523 K, as demonstrated by a cross-plot of their rates of formation in Figure 2b. Therefore, UCB-3 can be considered a drop-in replacement for Al-MCM-22 because it maintains a stable selectivity profile with time-on-stream, which is similar to fresh Al-MCM-22, while exhibiting a greater catalytic activity per gram and per acid site.

■ ASSOCIATED CONTENT

Supporting Information

Powder X-ray diffraction (PXRD) patterns; N_2 gas adsorption/desorption isotherms; TEM images; ^{29}Si MAS NMR spectra; ^{27}Al MAS NMR spectra. This material is available free of charge via the Internet at http://pubs.acs.org.

AUTHOR INFORMATION

Corresponding Authors

*E-mail: sizo@chevron.com.
*E-mail: askatz@berkeley.edu.

Present Address

[⊥]AMPAC Fine Chemicals, Rancho Cordova, CA.

Notes

The authors declare no competing financial interest.

ACKNOWLEDGMENTS

We are grateful to the Management and Transfer of Hydrogen via the Catalysis Program funded by Chevron Corporation for financial support. The NMR facility at Caltech was supported by the National Science Foundation (NSF) under Grant No. 9724240 and in part by the MRSEC Program of the NSF under Award No. DMR-520565. The STEM facility and research were funded by the Laboratory Directed Research and Development program at the Pacific Northwest National Laboratory. PNNL is operated by Battelle for the U.S. Department of Energy under Contract DE-AC05-76RL01830.

REFERENCES

(1) Corma, A. *Chem. Rev.* **1995**, *95*, 559−614.
(2) Degnan, T. F., Jr.; Smith, C. M.; Venkat, C. R. *Appl. Catal., A* **2001**, *221*, 283−294.
(3) Corma, A.; Martínez-Soria, V.; Schnoeveld, E. *J. Catal.* **2000**, *192*, 163−173.
(4) Inagaki, S.; Kamino, K.; Kikuchi, E.; Matsukata, M. *Appl. Catal., A* **2007**, *318*, 22−27.
(5) Gounder, R.; Iglesia, E. *Acc. Chem. Res.* **2011**, *45*, 229−238.
(6) Gounder, R.; Iglesia, E. *Chem. Commun.* **2013**, *49*, 3491−3509.
(7) Matias, P.; Lopes, J. M.; Laforge, S.; Magnoux, P.; Russo, P. A.; Ribeiro Carrott, M. M. L.; Guisnet, M.; Ramôa Ribeiro, F. *J. Catal.* **2008**, *259*, 190−202.
(8) Millini, R. In *Zeolites and Ordered Porous Solids: Fundamenals and Applications*; Martínez, C., Pérez-Pariente, J., Eds.; 2011 pp 227−233; Editorial Universitat Politècnica de València.
(9) Cejka, J.; Krejcí, A.; Zilková, N.; Kotrla, J.; Ernst, S.; Weber, A. *Microporous Mesoporous Mater.* **2002**, *53*, 121−133.
(10) Rigoreau, J.; Laforge, S.; Gnep, N. S.; Guisnet, M. *J. Catal.* **2005**, *236*, 45−54.
(11) Kim, W.; Kim, J.-C.; Kim, J.; Seo, Y.; Ryoo, R. *ACS Catal.* **2013**, *3*, 192−195.
(12) Jo, C.; Ryoo, R.; Zilková, N.; Vitvarová, D.; Cejka, J. *Catal. Sci. Technol.* **2013**, *3*, 2119−2129.
(13) Roth, W. J.; Cejka, J. *Catal. Sci. Technol.* **2011**, 43−53.
(14) Corma, A.; Diaz, U.; Fornés, V.; Guil, J. M.; Martínez-Triguero, J.; Creyghton, E. J. *J. Catal.* **2000**, *191*, 218−224.
(15) Corma, A.; Fornés, V.; Martínez-Triguero, J.; Pergher, S. B. *J. Catal.* **1999**, *186*, 57−63.
(16) Corma, A.; Fornes, V.; Pergher, S. B.; Maesen, T. L. M.; Buglass, J. G. *Nature* **1998**, *396*, 353−356.
(17) Van Den Brink, P. J.; Corma, A.; Creyghton, E. J.; Fornés, V.; Martinez, V. Aromatics Alkylation. U.S. Patent 6,855,855; February 15, 2005.
(18) Ramos, F. S. O.; de Pietre, M. K.; Pastore, H. O. *RSC Adv.* **2013**, *3*, 2084−2111.
(19) Maheshwari, S.; Jordan, E.; Kumar, S.; Bates, F. S.; Penn, R. L.; Shantz, D. F.; Tsapatsis, M. *J. Am. Chem. Soc.* **2008**, *130*, 1507−1516.
(20) Maheshwari, S.; Martínez, C.; Portilla, M. T.; Llopis, F. J.; Corma, A.; Tsapatsis, M. *J. Catal.* **2010**, *272*, 298−308.
(21) Archer, R. H.; Carpenter, J. R.; Hwang, S.-J.; Burton, A. W.; Chen, C.-Y.; Zones, S. I.; Davis, M. E. *Chem. Mater.* **2010**, *22*, 2563−2572.
(22) Archer, R. H.; Zones, S. I.; Davis, M. E. *Microporous Mesoporous Mater.* **2010**, *130*, 255−265.
(23) Ogino, I.; Eilertsen, E. A.; Hwang, S.-J.; Rea, T.; Xie, D.; Ouyang, X.; Zones, S. I.; Katz, A. *Chem. Mater.* **2013**, *25*, 1502−1509.
(24) Olah, G. A.; Olah, J. A.; Ohyama, T. *J. Am. Chem. Soc.* **1984**, *106*, 5284−5290.
(25) Allen, R. H.; Yats, L. D. *J. Am. Chem. Soc.* **1961**, *83*, 2799−2805.
(26) Rodewald, P. G. Silica-modified catalyst and use for selective production of *para*-dialkyl substituted benzenes. U.S. Patent 4,465,886; August 4, 1984.
(27) Rodewald, P. G. Silica-modified catalyst and use for selective production of para-dialkyl substituted benzenes. U.S. Patent 4,477,583, October 16, 1984.
(28) Chang, C. D.; Shihabi, D. S. Catalyst and process for the selective production of para-dialkyl substituted benzenes. U.S. Patent 5,243,117; September 7, 1993.
(29) Thiele, E. W. *Ind. Eng. Chem.* **1939**, *31*, 916−920.
(30) Zhang, X.; Liu, D.; Xu, D.; Asahina, S.; Cychosz, K. A.; Agrawal, K. V.; Al Wahedi, Y.; Bhan, A.; Al Hashimi, S.; Terasaki, O.; Thommes, M.; Tsapatsis, M. *Science* **2012**, *336*, 1684−1687.